Available online at www.sciencedirect.com
SCIENCE DIRECT
Journal of Catalysis 241 (2006) 389–399
JOURNAL OF CATALYSIS
www.elsevier.com/locate/jcat

Reaction of NO and O_2 to NO_2 on Pt: Kinetics and catalyst deactivation

S.S. Mulla [a], N. Chen [a], L. Cumaranatunge [a], G.E. Blau [a], D.Y. Zemlyanov [a], W.N. Delgass [a], W.S. Epling [b], F.H. Ribeiro [a,*]

[a] *School of Chemical Engineering, Purdue University, 480 Stadium Mall Drive, West Lafayette, IN 47907-2100, USA*
[b] *Department of Chemical Engineering, University of Waterloo, 200 University Ave. West, Waterloo, Ontario N2L 3G1, Canada*

Received 24 January 2006; revised 3 May 2006; accepted 8 May 2006

Available online 13 June 2006

Abstract

The kinetics of NO oxidation was determined on two Pt catalysts with average particle sizes of 2.4 nm (fresh) and 7.0 nm (sintered). The degree of surface oxidation after reaction, as measured by CO titration and XPS, determined the surface reactivity. The turnover rate (TOR) for NO oxidation at 300 °C with 300 ppm of NO, 170 ppm of NO_2, 10% of O_2, and the balance N_2 and at atmospheric pressure on a Pt/Al_2O_3 catalyst with a Pt particle size of 2.4 nm was 3.5×10^{-3} $mol_{NO}/(mol_{Pt}\,s)$. On the sintered catalyst, the TOR was 14.7×10^{-3} s^{-1}, a four-fold increase with respect to the fresh one. Measuring the rate of reaction on the fresh catalyst under a set of experimental conditions obtained using the central composite design statistical method, in which the interaction among the variables temperature and species concentration can be tested, confirmed the assumption in our previously published results that there is no interaction among the variables. The reaction was nearly first order with respect to NO and O_2 and nearly negative first order with respect to NO_2, and the apparent activation energy (E_a) was 81.8 ± 5 kJ mol^{-1}. With respect to the fresh catalyst, the sintered catalyst showed a similar E_a (80.9 ± 5 kJ mol^{-1}) and apparent reaction orders for NO and NO_2, with a lower O_2 order (0.7 ± 0.04). After the NO oxidation reaction attained steady state, both fresh and sintered catalysts showed an average oxygen uptake of about 1.5 times the number of Pt surface atoms. When the oxygen uptake was increased to the equivalent of two oxygen atoms per surface Pt by a different pretreatment, the NO oxidation TOR decreased by 85% with respect to the original steady-state level. XPS measurements suggested that over-oxidation of Pt was concomitant with this TOR decrease. Titration studies of surface oxygen using CO suggested that the rate of CO_2 formation was also higher on larger Pt particles.

Keywords: Kinetics of NO oxidation on Pt; Effect of particle size; Catalyst deactivation; NO_2 inhibition of NO oxidation

1. Introduction

New regulations imposed by the EPA [1] require reduction of NO_x emissions in the exhaust of lean-burn diesel engines. NO_x abatement techniques under development are based on two different approaches. The first is the continuous selective catalytic reduction (SCR) of NO_x with either unburned hydrocarbons (HC) from the fuel or with ammonia or urea injected into the engine exhaust. It has been proposed that the oxidation of NO in the exhaust to NO_2 over noble metal sites substantially increases the rate and selectivity of HC-SCR [2–6]. The second approach for NO_x abatement is the NO_x storage/reduction (NSR) technology pioneered by Toyota for mobile applications [7]. The catalyst used for the NSR process comprises a noble metal component that can catalyze oxidation and reduction reactions (e.g., Pt) and a NO_x storage component (typically alkali or alkaline earth metals, e.g., K or Ba). During lean operation, NO in the exhaust is oxidized to NO_2 over the noble metal component, whereas NO_2 and NO are stored as nitrates or nitrites on the storage component. The oxidation of NO in the exhaust to NO_2 is found to substantially increase the NSR catalyst performance, because storage of NO_2 is more facile than that of NO over these catalysts [8–14]. As the trap saturates and loses its storage capacity, it becomes necessary to regenerate it by providing a reducing atmosphere in which the stored NO_x is released and subsequently reduced to N_2 over noble metal sites. The NSR catalyst is used with an engine that operates

* Corresponding author. Fax: +1 765 494 0805.
E-mail address: fabio@purdue.edu (F.H. Ribeiro).

0021-9517/$ – see front matter
doi:10.1016/j.jcat.2006.05.016

alternately under lean- and rich-burn conditions to provide regeneration.

In addition, the oxidation of NO to NO_2 is a key reaction in the continuously regenerating trap (CRT®) for soot removal [15]. In this case, the strongly oxidizing nature of NO_2 is used to continuously oxidize the soot collected on a diesel particulate filter at temperatures much lower than those required with oxygen alone. The NO_2 is reduced to NO, which is then reoxidized to NO_2 over a Pt catalyst.

Thus, the oxidation of NO to NO_2 over Pt is an important step in several after treatment reactions. Previously, NO oxidation on supported Pt has been studied in experiments containing only NO and O_2 as reactants [16–19] and in the presence of SO_2 [20–22], water [6,23,24], and hydrocarbons [25,26]. Calculations using kinetic modeling [17,27,28] and ab initio kinetic Monte Carlo simulation [29–32] have also been conducted. However, most studies to date have not considered the influence of the product NO_2 on the rate of oxidation of NO. Recent studies have shown that the oxidation of NO is inhibited by the reaction product NO_2 on Pt supported by both γ-Al_2O_3 [33] and SiO_2 [6]. The NO oxidation turnover rate (TOR) is known to be a function of Pt particle size, with larger Pt particles giving higher rates on both Al_2O_3 [16,20,26,34,35] and SiO_2 [20,26,35] supports. Xue et al. [20] found this size dependence to be strong on Pt/SiO_2 compared with Pt/Al_2O_3 and found no size dependence on Pt/ZrO_2, although the presence of SO_2 in their studies may affect the trends. The catalyst support was also found to influence the rate of oxidation of NO to NO_2, with SiO_2-supported Pt exhibiting higher rates than Pt on Al_2O_3 or ZrO_2 [20,35].

Another factor that may influence the activity of platinum is its interaction with oxygen by either chemisorption or oxidation. Ovesson et al. [31], in a theoretical study, showed that NO oxidation is not an inherent property of the Pt catalyst itself, being in fact inhibited (endothermic) on Pt(111) by the strong oxygen–platinum bonds, and becomes exothermic only at sufficiently high oxygen coverage. Fridell et al. [36] suggested Pt-oxides formation as a possible reason for the decreased oxidation activity of a $Pt/BaO/Al_2O_3$ NO_x storage catalyst. Kieken et al. [29] performed simulations of the steady-state NO decomposition to N_2 in excess oxygen on Pt–Au (100) alloy surfaces and found that a decrease in the oxygen binding energy led to an increase in the TOR. Yazawa et al. [37] studied propane combustion and attributed the decrease in the propane conversion with time to the oxidation of Pt on both Pt/SiO_2–Al_2O_3 and Pt/ZrO_2 catalysts. Platinum oxides formation has also been observed during CO oxidation on Pt/SiO_2 [38], Pt(110) [39], and Pt(100) [40]. This latter study also linked the decreased catalytic activity with time on stream to the formation of surface oxide species [40]. The Pt–O interactions have also been found to influence the activity of supported Pt catalysts for the combustion of xylenes [41] and methane [42].

In the present study, we investigate the kinetics of the NO oxidation reaction on two Pt/Al_2O_3 catalysts having different Pt dispersions or particle sizes. An experimental design using statistical methods (central composite design) varied the species concentrations and the temperature simultaneously to measure the interaction among these variables. The results support the previously published kinetic results [33] obtained by changing one variable (temperature or concentration) while keeping the others constant, the one-at-a-time method. Another set of one-at-a-time variation experiments is used to study the reaction kinetics on a catalyst having a lower Pt dispersion. Flow reactor experiments and XPS measurements are used to monitor the decrease in conversion of the catalysts under reaction and other oxidizing conditions. Strong chemisorption of oxygen on Pt or Pt oxidation are suggested as potential causes of catalyst deactivation.

2. Experimental

2.1. Catalysts

The Pt/Al_2O_3 catalyst used in this study was supplied by EmeraChem in monolithic form. Based on a known liquid uptake of bare monolith, the appropriate amount of γ-Al_2O_3 was mixed as an aqueous slurry. The bare monolith was dipped into this slurry, drained, dried, and then calcined at 500 °C for 1 h. The monolith was then dipped into the Pt-containing aqueous solution such that a final Pt loading of approximately 50 g ft^{-3} of monolith was attained. The Pt salt precursor was amine-based.

The monolith had a Pt loading of ca. 0.3 wt% (per total monolith weight) and a cell density of 200 channels/in^2. The percentage of metal exposed or metal dispersion, defined as the ratio of the number of surface Pt atoms to the total number of Pt atoms, measured by H_2–O_2 titration [43], was 42% for the fresh monolith. Two 1-inch-long monolithic samples, both weighing ca. 3 g and having a cross-section of 60 cells, were used for the experiments. One of the samples was heat treated in dry air at 600 °C for 6 h to increase the Pt particle size (or to decrease the dispersion); we call it the "sintered catalyst." The other sample was used without any heat treatment (i.e., Pt dispersion of 42%); we call it the "fresh catalyst."

2.2. Experimental setup

The experiments were performed in a bench-top flow stainless steel reactor. High-temperature Zetex insulation was wrapped around the catalyst sample, and the assembly was placed in the reactor tube. The insulation material blocked the space between the monolith and the wall of the reactor, minimizing the gas flow bypassing the catalyst. Glass beads were placed upstream of the catalyst sample to ensure mixing and uniformity of the gas flow. The reactor was placed inside a temperature-controlled furnace. To minimize temperature gradients before entering the reactor, the inlet gas was passed through a separate preheater consisting of a coiled $\frac{1}{4}$-inch-diameter tube inside a furnace. Thermocouples were placed 6 mm before and after the catalyst sample to verify inlet and outlet gas temperatures. A reactor bypass loop after the preheater, and thus at the reactor conditions, was used to verify the nominal inlet concentrations of NO and NO_2 after each catalytic rate measurement. The gas-phase rates were negligible compared with the catalytic ones.

All TOR calculations were done relative to the gas-phase bypass concentrations, and hence reflected only the reaction over the catalyst and not the gas phase.

2.3. Reaction kinetics measurements

The NO oxidation apparent activation energy and reaction orders with respect to NO, O_2, and NO_2 were estimated from data for both fresh and sintered catalysts. Before the experiments were performed, the catalyst samples were pretreated at 150 °C with 10% O_2 in N_2 for 1 h, followed by reduction with 0.5% H_2 in N_2 for 1.5 h with a constant total flow rate of 6.5 L min^{-1}. The reactor was operated in a differential manner by restricting the NO conversion to <10% and by using excess NO_2 in the feed so that the contribution of the NO_2 formed to the total NO_2 concentration was negligible. The NO and NO_x ($NO + NO_2$) concentrations in the outlet gas were detected with a chemiluminescence detector (California Analytical Instruments HCLD 400). The data reported here were taken after the catalyst was on stream for at least 1 h and steady state was reached.

On the sintered catalyst, the estimate of the apparent activation energy was determined from data collected by randomly varying the temperature between 279 and 300 °C, while maintaining the feed composition at 300 ppm NO, 170 ppm NO_2, 10% O_2, and balance N_2 and the total flow rate at 6.6 L min^{-1}. Similar one-at-a-time variation experiments were conducted to estimate the effect of reactant and product concentrations on the NO oxidation rate. The concentrations of the various species were varied over the ranges 80–480 ppm for NO, 10–25% for O_2, and 100–240 ppm for NO_2, at a constant baseline temperature of 300 °C. To measure reproducibility and any catalyst deactivation, the last point in a sequence was a repeat of the first point. The actual estimates and their confidence limits for apparent reaction orders and activation energy were obtained by a log-linear least-squares analysis assuming a constant error in the oxidation rate.

For the fresh catalyst, a kinetic model has been postulated and parameter estimates generated from similar one-at-a-time variation-type experiments [33]. To confirm these results, an additional set of experiments was generated for the fresh catalyst using a central composite design [44]. Part of the central composite design varies all four factors (temperature and the concentrations of NO, O_2, and NO_2) simultaneously, which allows the analysis to capture any interactions between the parameters (discussed in Section 3.1). Another part of this design uses a one-at-time variation approach to measure extreme points around the base or center point. The complete design consisted of 32 experiments in which the runs from the above two parts were mixed randomly and the four factors were varied over the ranges 240–320 °C, 100–500 ppm NO, 3–25% O_2, and 25–300 ppm NO_2 and included 8 repeat points at approximately the center of these ranges (285 °C, 300 ppm NO, 16.3% O_2, and 120 ppm NO_2). By placing the center points at constant time intervals throughout the experiments, it was possible to measure reproducibility as well as monitor the deactivation of the catalyst over the life of the program. Care was taken to ensure that these statistically designed experiments remained in the differential reactor regime.

The experiments were conducted with a total flow of approximately 6.6 L min^{-1}. The criteria suggested by Dekker et al. [45] were used to check external heat and mass transfer limitations. The Carberry number (Ca) and the parameter for external heat transfer limitation—given as $|(k_g(-\Delta H)C_b/hT_b)\gamma Ca|$, where k_g and h are extraparticle mass and heat transfer coefficients respectively; C_b and T_b are steady-state bulk concentration and temperature, respectively; and $\gamma = E_a/RT_b$—were of the order of 10^{-4} ($\ll 0.05$), suggesting negligible transport effects.

2.4. XPS studies

The XPS study was done in a Perkin–Elmer PHI 5300 system. Sample treatment was performed in the reaction cell attached to the system. The samples could be exposed to various gas mixtures at 1 atm and transferred to the UHV chamber without being exposed to ambient air. About 100 mg of powdered catalyst (either fresh or sintered) was loaded into a cylindrical mold and made into a pellet 1.42 cm in diameter and 1.3 mm thick, using a bench-top hydraulic press under 5000 psi pressure. The analysis was performed on both catalysts after each of the following pretreatments: (i) reduction in 5% H_2/N_2 at 300 °C for 1 h, then cooling in N_2 to room temperature, followed by either (ii) exposure to 150 ppm NO/air at 300 °C for 1 h, then cooling in the same gas mixture to room temperature, or (iii) exposure to 1% NO_2/air at 300 °C for 1 h, then cooling in the same gas mixture to room temperature. The XPS spectra were recorded using nonmonochromatic Al-K_α radiation. The binding energy (BE) values referred to the Fermi level were calibrated using the Al 2p energy of 74.7 eV [46]. The X-ray power was 150 W, and the pass energy for the analysis was 8.95 eV for all measurements. The XPS spectra were fitted by CasaXPS software (Casa Software Limited) assuming line shape to be a Doniach–Sunjic function [47] with Gaussian and Lorentzian contributions of 70 and 30%, respectively. The Shirley-type background [48] was subtracted. The Pt 4f doublet separation was fixed at 3.3 eV [46], and the $4d_{3/2}$:$4d_{5/2}$ and the $4f_{5/2}$:$4f_{7/2}$ area ratios were set to 0.67 and 0.75, respectively.

2.5. Oxygen uptake measurements by CO titration

The uptake of oxygen by the catalysts exposed to various pretreatments was determined using the same reactor setup used for the kinetic measurements described above. The catalysts were subjected to the following pretreatments: (1) oxygen exposure at room temperature with 15% O_2/N_2 (ca. 100 Torr O_2) for 30 min, (2) NO oxidation reaction mixture exposure under standard conditions (300 °C, 300 ppm NO, 170 ppm NO_2, 10% O_2, balance N_2) for 1.5 h, and (3) catalyst deactivating mixture exposure with 1000 ppm NO_2, 10% O_2, and a balance of N_2 at room temperature overnight, followed by NO oxidation TOR measurement again under the standard conditions noted above.

After each of these pretreatments, the flow was switched to He (488 cm^3 min^{-1}) to purge out any residual gases from the

pretreatments, and the reactor temperature was set to 160 °C. Some of the weakly bound oxygen could desorb during the purging treatment, but this amount was small, as evidenced by the agreement on the fresh catalyst between the Pt area measured by H_2–O_2 titration and this method (discussed in Section 3.3). At this temperature, the flow was changed to 2% CO/He (488 $cm^3\,min^{-1}$), and simultaneously the exit gases were analyzed in an FTIR gas analyzer (Thermo Electron Corp., Nicolet Antaris IGS) for CO_2. The CO_2 trace was followed until it decreased to below detection (typically about 5 min). The resulting CO_2 trace was integrated and, by assuming the reaction stoichiometry $CO + O = CO_2$, the total amount of oxygen on Pt was calculated.

3. Results

3.1. NO oxidation kinetics results on the fresh Pt/Al_2O_3 catalyst

A nonlinear least squares analysis was used to fit the data from the designed experimental program on the fresh catalyst (described in Section 2.3), excluding the rate data that showed catalyst deactivation (described later), to a power rate law model of the form

$$r_f = \exp\left(A - \frac{E_a}{RT}\right)[NO]^{\alpha}[O_2]^{\delta}[NO_2]^{\gamma}, \quad (1)$$

with r_f as the forward rate of reaction (s^{-1}), $\exp(A)$ as the pre-exponential factor (s^{-1}), E_a as the apparent activation energy ($J\,mol^{-1}$), T as the temperature (K), $[C_i]$ as the gas-phase volume fraction of species C_i in the reactor effluent, and α, δ, and γ as the apparent forward reaction orders. The rates were expressed as TORs, defined as moles of NO reacted per second per mole of surface Pt. The forward rates (r_f) were calculated from the measured overall rates (r_{ov}) using the expression

$$r_f = \frac{r_{ov}}{(1-\beta)}, \quad (2)$$

where β is the approach to equilibrium given as

$$\beta = \frac{[NO_2]}{K[NO][O_2]^{1/2}}, \quad (3)$$

with K as the equilibrium constant. The β values in our experiments ranged from 0.02 to 0.17, indicating that the reaction was far from equilibrium. The data were fit using the statistical software JMP 5.0.1 (SAS Institute, Inc.), assuming that the errors in the response (i.e., TOR values) are normally and independently distributed and homoscedastic (i.e., do not depend on the response). The pre-exponential factor obtained as a result of this fit was $\exp(15.1 \pm 1.03)\ s^{-1}$. Table 1 gives the parameter estimates for E_a and the apparent reaction orders, along with the log-linear least squares parameter estimates generated previously [33]. In both cases, there is a near-first-order dependence of the TOR on O_2 and NO concentrations and a near-negative first-order dependence on NO_2 concentration with an apparent activation energy of $81.8 \pm 5\ kJ\,mol^{-1}$ over the temperature and the concentration ranges studied (240–320 °C, 100–500 ppm NO, 3–25% O_2, 25–300 ppm NO_2). The observed rates and the model calculated rates and their 95% confidence intervals are compared in Fig. 1. Noting that the results from Ref. [33] (first row of Table 1) were obtained from the one-at-a-time approach (where the apparent reaction orders were measured only at 300 °C, and the E_a was measured only at 300 ppm NO, 170 ppm NO_2, 10% O_2, balance N_2), whereas the results in this work were obtained by simultaneously varying the temperature and concentrations over the above-mentioned ranges, the similarity between the results of these two experimental designs (central composite vs. traditional one-at-a-time variations), as shown in Table 1, validates the assumption that the apparent ki-

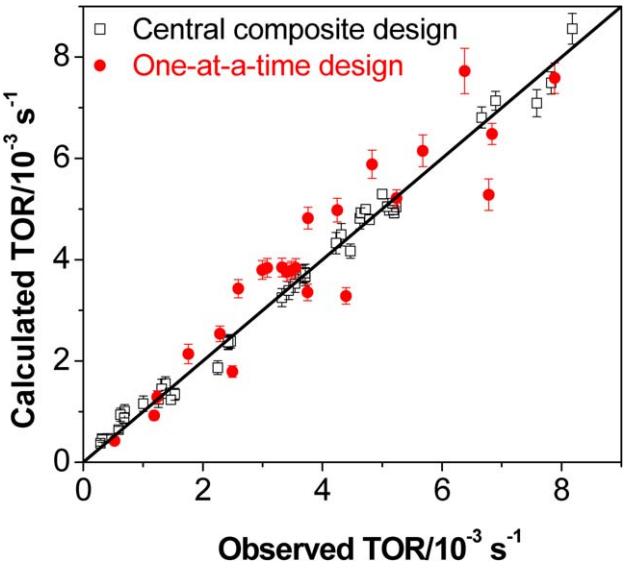

Fig. 1. Comparison between the observed turnover rates and the model calculated rates for fresh Pt/Al_2O_3 catalyst. The 95% confidence intervals of the calculated rates are also shown. The open squares are the data from the central composite design while the solid circles show the model predictions for the rates observed during the one-at-a-time variation experiments.

Table 1
Summary of the NO oxidation reaction kinetics on fresh and sintered Pt/Al_2O_3 catalysts

Catalyst	PME[d] (%)	E_a ($kJ\,mol^{-1}$)	NO order	O_2 order	NO_2 order	TOR[c] ($\times 10^{-3}\ s^{-1}$)	Ref.
Fresh[a]	42	82.6±9	1.05 ± 0.08	1.03 ± 0.08	−0.92 ± 0.07	3.5 ± 0.1	[33]
Fresh[b]	42	81.8±5	1.09 ± 0.07	0.86 ± 0.06	−0.85 ± 0.06	3.9 ± 0.2	This work
Sintered	15	80.9±5	1.12 ± 0.08	0.69 ± 0.04	−0.89 ± 0.06	14.7 ± 0.4	This work

[a] Kinetic parameters obtained by varying one factor (T, [NO], [O_2] or [NO_2]) at a time and using log linear least-squares fit, as detailed in Ref. [33].
[b] Kinetic parameters obtained from the simultaneous variations in temperature and species concentrations and using nonlinear least-squares fit.
[c] TOR at 300 °C, 300 ppm NO, 170 ppm NO_2, 10% O_2, balance N_2.
[d] PME, percentage of metal exposed.

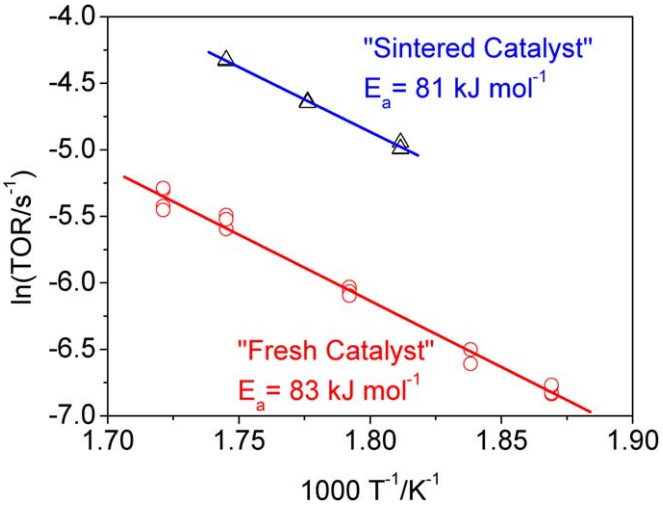

Fig. 2. Arrhenius plot for NO oxidation on the fresh and sintered Pt/Al_2O_3 catalysts assuming a differential reactor. Feed: 300 ppm NO, 10% O_2, 170 ppm NO_2, balance N_2.

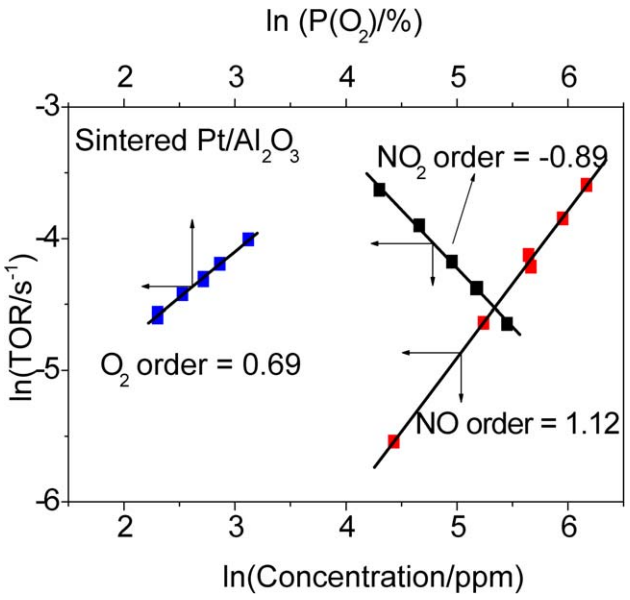

Fig. 3. NO oxidation turnover rate (TOR) dependence on O_2, NO and NO_2 concentrations at 300 °C for a sintered Pt/Al_2O_3 catalyst. Feed for NO order: 170 ppm NO_2, 10% O_2, 80–480 ppm NO; feed for NO_2 order: 10% O_2, 300 ppm NO, 100–240 ppm NO_2, feed for O_2 order: 300 ppm NO, 170 ppm NO_2, 10–25% O_2. All feeds have N_2 as the balance gas.

netic parameters of NO oxidation reaction are independent of one another. In other words, the temperature dependence obtained at a fixed species concentration used in Ref. [33] is also valid over a range of concentrations noted above, and the apparent reaction orders obtained at one temperature (300 °C) hold over a range of temperatures.

3.2. NO oxidation kinetics results on the sintered Pt/Al_2O_3 catalyst

Fig. 2 shows the variation in NO oxidation reaction rate with temperature over the sintered Pt/Al_2O_3 catalyst. Fig. 3 shows the effects of reactant and product concentrations on the NO oxidation TOR at 300 °C for the sintered catalyst. These results are summarized in Table 1. Similar to the findings for the fresh catalyst, the rate of NO oxidation had a near-first-order dependence with respect to NO concentration and was close to negative first-order with respect to the product NO_2 concentration. Thus, NO_2 inhibited NO oxidation on the sintered Pt/Al_2O_3 catalyst as well. There appeared to be no significant difference between the estimated apparent activation energies for the two catalysts; however, the apparent O_2 order on the sintered catalyst was 0.7, significantly lower than the near-first-order O_2 dependence obtained on the fresh catalyst.

For comparison, Table 1 also includes NO oxidation TORs on fresh and sintered Pt/Al_2O_3 catalysts under the same reaction conditions. The TOR was found to be significantly higher on the sintered catalyst. This is also evident from the Arrhenius plots in Fig. 2. At the standard conditions (300 °C, 300 ppm NO, 10% O_2, 170 ppm NO_2, balance N_2), the TOR on the sintered catalyst was ca. 4 times higher than that on the fresh catalyst. As will be shown later, this sintered catalyst had an average Pt particle size of about 7 nm (compared with 2.4 nm for the fresh catalyst). This is consistent with the observations made by several other groups regarding larger Pt particles exhibiting higher TORs for NO oxidation than smaller particles [16,20,26,34,35].

3.3. Deactivation of the Pt/Al_2O_3 catalyst for NO oxidation

As mentioned earlier, both the fresh and sintered catalysts were found to deactivate for the NO oxidation reaction, but only during changes in conditions, not during reaction. Deactivation of Pt for NO oxidation has also been reported previously [6,24,34]. Under our experimental conditions, the catalysts showed stable TORs during reaction (which typically lasted 6–7 h). After reaction, the sample was cooled to room temperature under N_2 flow. When the catalyst was again brought to reaction conditions, it showed varied degrees of deactivation, which was independent of the variation in the reaction temperature or species concentration under reaction conditions. These deactivated catalysts would again yield stable rates (although lower than their original values seen earlier) under reaction conditions but would deactivate further on the shutdown procedure. The catalyst deactivation during cooling to room temperature in N_2 flow suggested that traces of the oxidizing reaction gas mixture (containing NO, O_2, and NO_2) left in the system's dead volume could possibly be the source of deactivation. In fact, it was found later that when the catalysts were pretreated with a strong oxidizing mixture containing 1000 ppm NO_2, 10% O_2, and balance N_2 overnight at room temperature, the catalysts deactivated, with the TOR decreasing to about 15% of the original rates shown in Table 1. However, we found the deactivation to be completely reversible. Reducing these deactivated catalysts with 2% CO/He at 160 °C would regenerate them completely in about 3 min, and the oxidation rates would return to their original levels seen before catalyst deactivation. Similar regeneration results were obtained with a treatment using 0.5% H_2/N_2.

Table 2
XPS Pt $4f_{7/2}$ and $4d_{5/2}$ peak positions, FWHM and peak areas for the fresh and sintered catalysts

Treatment	Catalyst	Pt $4f_{7/2}$			Pt $4d_{5/2}$		
		BE (eV)	FWHM (eV)	Relative area[d]	BE (eV)	FWHM (eV)	Relative area[d]
H_2/N_2[a]	Fresh	71.7	2.5	0.38	315.1	4.9	0.28
	Sintered	71.3	2.4	0.16	314.6	4.4	0.13
NO/air[b]	Fresh	72.2	2.6	0.32	315.8	4.9	0.21
	Sintered	71.8	2.3	0.15	315.4	5.0	0.11
NO_2/air[c]	Fresh	72.4	2.8	0.36	316.2	5.7	0.27
	Sintered	71.9	2.0	0.13	315.6	3.9	0.10

[a] Reduction in 5% H_2/N_2 at 300 °C for 1 h, then cool in N_2 to room temperature.
[b] Exposure to 150 ppm NO/air at 300 °C for 1 h, then cool in the same gas mixture to room temperature.
[c] Exposure to 1% NO_2/air at 300 °C for 1 h, then cool in the same gas mixture to room temperature.
[d] Ratio of the peak area to that of the corresponding Al 2p peak.

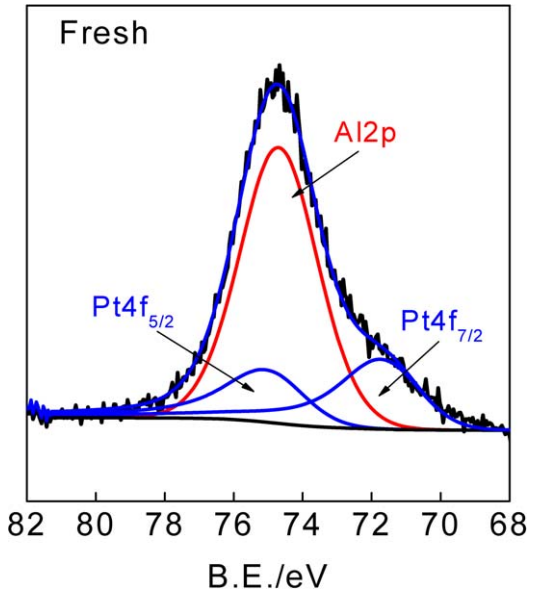

Fig. 4. XPS Pt 4f spectra and the curve fit obtained on the fresh catalyst. The catalyst was reduced in 5% H_2/N_2 at 300 °C for 1 h, then cooled in N_2 to room temperature.

The catalyst samples were also analyzed with XPS after being treated with H_2, NO/air, and NO_2/air, as described in Section 2.4. As an example, Fig. 4 shows the Pt 4f spectra along with the curve fit for the fresh catalyst after the H_2 pretreatment. Table 2 gives the positions, FWHM, and the peak areas relative to the Al 2p peak for the Pt $4d_{5/2}$ and Pt $4f_{7/2}$ peaks. The accuracy of determination of the binding energy is ±0.2 eV, and that of FWHM is ±0.4 eV. For the H_2-treated samples, the Pt 4d and 4f peaks were observed at higher binding energies compared with the respective Pt^0 values of 314.2 eV and 71.1 eV reported for Pt foils [49]. Such shifts toward high binding energies have been reported for Pt supported on alumina [34,49–51]. Moreover, the H_2-pretreated fresh catalyst (2.4 nm) had about 0.4–0.5 eV higher binding energy than the corresponding sintered catalyst with larger Pt particles (7 nm). Huizinga et al. [50] also found that the binding energy of Pt supported on alumina decreased as the Pt particles were sintered; they attributed this to the more effective screening of the core holes by the electrons of the neighboring atoms in larger particles. These binding energies thus correlate well with reported values for Pt^0 [49,50], indicating that the reduced samples contain mainly metallic platinum. For the NO/air and NO_2/air pretreated samples, which were also cooled in the respective pretreatment gas, the peaks were shifted even more toward higher binding energies, with the highest shifts seen for the NO_2/air pretreated samples. Moreover, for a given pretreatment, similar shifts were seen for both fresh and sintered catalysts. The relative intensities of the Pt peak to the Al peak were also higher for the fresh catalyst than for the sintered catalyst, further corroborating the presence of larger Pt clusters on the sintered catalyst.

To further understand the deactivation of Pt for the NO oxidation reaction, the uptake of oxygen by the fresh and sintered catalysts after they had been subjected to three distinct oxidation treatments (described in Section 2.5) was measured by a CO titration method at 160 °C. The integration of the CO_2 trace allowed the quantification of the oxygen uptake by the catalysts, with each CO_2 molecule formed corresponding to one atomic oxygen on the catalyst ($CO + O = CO_2$). Table 3 lists the amount of oxygen thus measured in units of mol g_{cat}^{-1}. The accuracy of oxygen uptake measurements is $\pm 1 \times 10^{-7}$ mol g_{cat}^{-1}. As noted by Benson and Boudart [43], the oxygen exposure at room temperature leads to a monolayer of adsorbed oxygen with an O/Pt_S ratio of unity. It was thus possible to calculate the surface Pt moles on the fresh and sintered catalysts from the CO titration after the room temperature oxygen exposure, and hence the Pt dispersion (ratio of surface Pt to total Pt) while the catalysts were in use. Knowing the total Pt content of the catalysts, this gave a Pt dispersion of 39% for the fresh catalyst, in good agreement with the 42% Pt dispersion that we obtained from the independent H_2–O_2 chemisorption measurement before use, as mentioned earlier. Likewise, for the sintered catalyst, the Pt dispersion was found to be 15% based on the CO titration results after this room temperature O_2 pretreatment. Fig. 5 shows the CO titration traces normalized by the corresponding surface Pt moles for the fresh and the sintered catalysts. The area under the normalized CO titration curve after pretreatment with O_2 is then made to be unity for both catalysts.

Table 3
Oxygen uptake of the fresh and sintered catalysts following various pretreatments

Catalyst	Uptake of atomic oxygen ($\times 10^{-6}$ mol g_{cat}^{-1})			PME based on O_2 pretreatment (%)
	Pretreatment with O_2[a]	Pretreatment with reaction mixture[b]	Pretreatment with deactivation mixture[c]	
Fresh	1.77	2.60	3.67	39
Sintered	0.67	0.97	1.33	15

[a] 15% O_2/N_2 at room temperature for 30 min.
[b] 300 ppm NO/170 ppm NO_2/10% O_2/N_2 at 300 °C for 1.5 h.
[c] 1000 ppm NO_2/10% O_2/N_2 at room temperature, overnight.

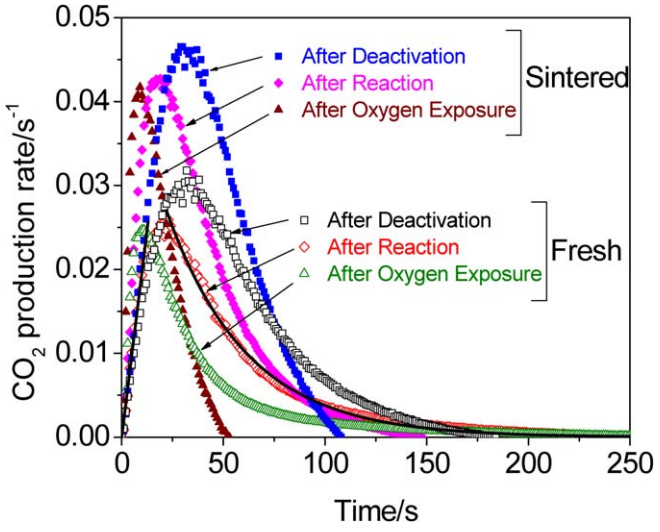

Fig. 5. Rate of CO_2 production on the fresh and sintered catalysts normalized by the corresponding surface Pt moles during the titration. Pretreatments: (i) O_2 exposure: 15% O_2/N_2 at room temperature for 30 min; (ii) NO oxidation reaction: 300 ppm NO/170 ppm NO_2/10% O_2/N_2, at 300 °C for 1.5 h; (iii) deactivation: 1000 ppm NO_2/10% O_2/N_2 at room temperature, overnight. Feed for titration: 2% CO/He, 488 cm^3 min^{-1}, 160 °C. The linear and the exponential fit to the titration curve of the fresh catalyst after NO oxidation reaction is also shown by a solid line.

4. Discussion

4.1. NO oxidation reaction kinetics

From Table 1, it can be seen that for the fresh and sintered catalysts with varying Pt dispersions or percentages of metal exposed, the activation energy and reaction orders for the NO oxidation reaction are similar except for the lower dependence on O_2 concentration seen for the sintered catalyst. The reaction mechanism that we proposed [33] to explain the observed apparent orders on the fresh catalyst is as follows:

$$\mathrm{NO} + * \overset{K_1}{\rightleftharpoons} \mathrm{NO}*, \tag{4}$$

$$\mathrm{NO_2} + 2* \overset{K_2}{\rightleftharpoons} \mathrm{NO}* + \mathrm{O}*, \tag{5}$$

$$\mathrm{O_2} + * \overset{k_3}{\rightarrow} \mathrm{O_2}*, \tag{6}$$

$$\mathrm{O_2}* + * \overset{k_4}{\rightarrow} 2\mathrm{O}*, \tag{7}$$

where $*$ denotes a Pt site and K_i and k_i denote the equilibrium constant and the rate constant of the ith step, respectively. Step (6) was proposed as the rate-determining step (RDS), and O$*$ as the most abundant surface intermediate [17,27,52], with steps (4) and (5) in quasi-equilibrium. Note that step (5) is not an elementary step, but rather is a combination of NO_2 adsorption and dissociation steps, both of which are assumed to be in quasi-equilibrium. The rate expression is then obtained as

$$r = \{k_3[\mathrm{L}]\}\frac{[\mathrm{O_2}]}{1 + \frac{K_2[\mathrm{NO_2}]}{K_1[\mathrm{NO}]}}, \tag{8}$$

which, under the limiting condition of high O$*$ coverage, takes the form

$$r = \left\{\frac{k_3[\mathrm{L}]K_1}{K_2}\right\}\frac{[\mathrm{NO}][\mathrm{O_2}]}{[\mathrm{NO_2}]}. \tag{9}$$

Here [L] denotes the total surface concentration of active metal sites. Eq. (9) has the same concentration dependence (apparent reaction orders) as seen in our experiments for the fresh catalyst.

The TORs on the sintered catalyst were found to be about 4 times higher than those on the fresh catalyst under identical conditions, as noted in Table 1. Such a dependence of TORs on Pt dispersion/particle size has been reported previously [16,20,26,34,35]. Although Xue et al. [20] found about a nine-fold increase in NO oxidation TOR in the presence of SO_2 at 300 °C on Pt/Al_2O_3 catalysts as the Pt particle size increased from 2.4 nm to 6.3 nm, Lee and Kung [16] reported a >100-fold greater TOR at 265 °C on a Pt/Al_2O_3 catalyst with a Pt particle size of ca. 23 nm compared with one with ca. 1.2 nm particles. We also compared our TORs with those found in the literature. Table 4 shows a compilation of the rate data in the literature obtained by integrating the data provided in the original papers using our kinetic model and normalizing to our reaction conditions. Our TOR fits well with the observed trend of increasing rate with increasing Pt particle size. Moreover, the TOR on our sintered catalyst is in good agreement with the rate reported by Despres et al. [6] on their Pt/SiO_2 catalyst with nearly the same Pt particle size (ca. 7 nm).

Some researchers [34,35] have attributed the decreased TOR for NO oxidation with decreasing Pt particle size (or increasing Pt dispersion) to the resistance/stability of larger particles toward platinum oxides formation (which show lower rates for NO oxidation than those on metallic platinum) or to their weak oxygen adsorption ability compared with smaller particles, based on their TPD measurements and flow reactor experiments. Similar influence of Pt particle size on catalyst activity has been observed for other reactions, including the combustion of xylenes on carbon aerogel-supported Pt catalysts [41] and

Table 4
Literature values for turnover rates of NO oxidation to NO_2 on Pt, revised from [23]

Catalyst	Pt loading (wt%)	Pt particle size[b] (nm)	Turnover rate[a] ($\times 10^{-2}$ s^{-1})	Ref.
Pt/Al_2O_3	0.27	1.2	0.23	[16]
Pt/Al_2O_3 (fresh)	0.3	2.4	0.35	This work
Pt/Al_2O_3 (sintered)	0.3	7	1.5	This work
Pt/SiO_2	2.5	7	4.2[c]	[6]
Pt/Al_2O_3	2.3	22	16	[17]
Pt/Al_2O_3	2	200	25	[27]

[a] Rates per unit of surface Pt atom corrected to 300 °C, 300 ppm NO, 170 ppm NO_2, 10% O_2, balance N_2.
[b] Calculated using d (nm) $\approx 1/$(Pt dispersion), except for Refs. [6,27], where XPS intensities and SEM micrograph were used, respectively.
[c] 5% water was also present in the feed.

methane combustion on Pt/Al_2O_3 [42]. Those authors [41,42] observed that the lower TOR of small Pt particles was due to the stronger Pt–O bonds formed by Pt during the reaction. Similarly, Boudart et al. [53] found a marked susceptibility to oxygen poisoning for well-dispersed Pt catalysts compared with sintered, less dispersed catalysts or Pt foil while measuring the TOR for cyclopropane hydrogenation at 0 °C. Hartmann et al. [38] also found that small Pt clusters oxidize more easily than larger particles. Putna et al. [54] suggested that the interaction of oxygen with small Pt particles is stronger than that on the larger particles, or that the repulsive interactions between oxygen adatoms are less important on the surfaces of the small particles. Small Pt particles should have a higher concentration of low-coordination sites, whereas for the larger particles, the concentration of thermodynamically favored, closely packed (111) sites should be greater. Brown et al. [55] have reported a lower O_2 initial sticking probability (0.06 vs. 0.34), a lower Pt–O bond energy (405 vs. 427 kJ mol^{-1}), and a lower O_2 initial adsorption heat (316 vs. 360 kJ mol^{-1}) on Pt(111) compared with Pt(110). Thus, the reason for the higher TORs for NO oxidation on larger Pt particles could be that, both thermodynamically and kinetically, the (111) surfaces may be more difficult to oxidize, or they may interact more weakly with oxygen than the more open surfaces.

4.2. Deactivation of Pt

During the flow experiments, the catalysts were found to give stable rates under reaction conditions but would deactivate when cooled under oxidizing conditions. The deactivated catalysts were found to regenerate when exposed to a reductant (CO or H_2). These observations suggest the oxidation of Pt as a possible reason for the observed deactivation. The shifts in the binding energy of Pt seen in the XPS spectra after similar pretreatments also indicate the oxidation of Pt. In a similar study, Despres et al. [6] also found a persistent deactivation of their Pt/SiO_2, Pt/Al_2O_3, and Pt/ZrO_2 catalysts for NO oxidation on pretreatment with a mixture of NO_2 and O_2 at 250 °C, but pretreatment with O_2/N_2 alone caused no change in the catalyst activity. The initial activity of the deactivated samples in that study was completely restored either by thermal regeneration in static air at 650 °C or by treatment with a reducing agent like NH_3 or NO in N_2 at 250 °C. Those authors also observed that temperatures below 650 °C were not sufficient to completely regenerate the catalysts thermally. Berry [56] showed that the oxide on the surface of Pt wire was thermodynamically stable at low temperatures and high oxygen pressures and that the temperature required for rapid dissociation of the oxide in 1 atm air was in the 600–650 °C range. This is consistent with our results showing that the catalysts deactivated by cooling under oxidizing conditions would not regenerate when reheated to our reaction temperature of 300 °C. Olsson and Fridell [34] also found an activity decrease with time during the NO oxidation reaction on Pt/Al_2O_3 catalyst for a feed containing a mixture of NO and O_2 in Ar at both 250 and 300 °C over a 3-h period, with more pronounced deactivation at 250 °C than at 300 °C. It must be mentioned again that, contrary to the observations of Olsson and Fridell [34], our Pt/Al_2O_3 catalyst showed no deactivation during the 6–7 h of reaction, as noted earlier. Olsson and Fridell also found that their Pt/Al_2O_3 catalyst deactivated for the dissociation of NO_2 to NO at 350 °C over a 3-h period. Treatment with O_2/Ar alone was also able to deactivate their catalyst, and cooling it in NO_2/Ar mixture resulted in its complete deactivation for the NO_2 dissociation reaction. The catalyst was partially regenerated by exposure to a NO and O_2 mixture. According to studies of NO oxidation and NO_2 dissociation [6,34], the presence of NO_2 promotes the oxidation of Pt particles and causes a decrease in catalytic activity. Those studies further showed the formation of platinum oxides (PtO, PtO_2) by XPS measurements, suggesting that this deactivation resulted from platinum oxides or strongly chemisorbed oxygen. Segner et al. [57] and Parker and Koel [58] demonstrated that NO_2 indeed is a very effective source of surface oxygen because of its high sticking coefficient. Based on the chemical shift, our XPS results also indicate a higher average oxidation state of Pt on catalyst deactivation (by NO_2 pretreatment) than after reaction. Even after deactivation, however, oxidation of the Pt did not go beyond PtO; if it had, then the PtO_2 binding energy shift of ca. 3 eV would have corresponded to a PtO_2 shoulder in the XPS spectra, which we would have been able to observe [6,34] but did not.

4.3. CO titration studies

CO titration experiments were used in this study to quantify the uptake of oxygen. The total amount of CO_2 formed on the fresh and sintered catalysts after various pretreatments (with oxygen, NO oxidation reaction mixture, and catalyst deactivation mixture containing 1000 ppm NO_2/10% O_2/N_2), which also equals the oxygen uptake quantities, are listed in Table 3

in moles per gram of catalyst. The CO titration experiment after the pretreatment with the deactivation mixture also served to regenerate the catalysts completely, as mentioned earlier.

Inspection of the oxygen uptake quantities in Table 3 reveals that after pretreatment with the reaction mixture, the oxygen uptake was ca. 1.5 times the oxygen uptake after room temperature O_2 exposure for both fresh and sintered catalysts. In other words, after the NO oxidation reaction, both catalysts showed oxygen uptakes about 1.5 times the amount of Pt on their respective surfaces. Likewise, after the pretreatment with the deactivation mixture (1000 ppm NO_2/10% O_2/N_2), after which the NO oxidation TOR under standard reaction conditions decreased from the original value by about 85%, the oxygen uptake increased to nearly twice that obtained on the catalyst surface after the pretreatment with oxygen. This suggests a similar uptake of oxygen by the fresh and the sintered catalysts, proportional to their exposed Pt surface area, after NO oxidation reaction and after their deactivation. The similar shifts in the Pt binding energy seen on the XPS for both the fresh and the sintered catalysts after pretreatments similar to those described above also support this observation. McCabe et al. [59] reported that the oxidizable fraction of Pt in a series of silica and alumina-supported Pt catalysts of widely varying Pt particle size was simply proportional to the fraction of surface Pt atoms. The location and chemical nature of the additional oxygen after reaction and deactivation were not determined. The XPS results support oxidation of Pt but to a lower oxidation state than PtO_2. The additional oxygen not used to further oxidize Pt could be located below the surface. Legare [60] showed by DFT calculations that no oxygen atomic adsorption on Pt(111) was stable beyond 0.5 ML, except by occupation of a subsurface site, and also that subsurface O species could be stable at temperatures below 700 K and O_2 pressures of $\leqslant 1$ bar. Weaver et al. [61] found using XPS that PtO_2 or an intermediate oxide (such as Pt_2O_3) was formed at oxygen coverage $>$ about 1 ML while studying the oxidation of Pt(111) by gas-phase oxygen atoms in ultra-high vacuum at 450 K. Yeh et al. [62,63] reported that the platinum-oxide species formed on Pt/Al_2O_3 by oxygen depends on the oxidation temperature, duration of oxidation, and Pt particle size. They found that chemisorbed oxygen, PtO, and PtO_2 were the dominant products at oxidation temperatures of 25, 300, and 500 °C, respectively, and that the chemisorbed oxygen at 25 °C could transform to PtO or PtO_2 when the duration of oxidation was changed from 2 h to $>$10 h [62]. In addition, the oxide formed at ca. 500 °C changed from PtO_2 to PtO as the Pt particle size changed from $<$1.3 nm to $>$2 nm [63]. McCabe et al. [59] also obtained similar results. On supported Pt particles $<$1.5 nm, the oxygen uptake corresponded to PtO_2, but for particles $>$4 nm, the oxygen film was characteristic of chemisorbed oxygen rather than platinum oxide. These results, combined with our XPS and CO titration measurements, indicate an evolution of the oxygen species from the chemisorbed state toward PtO on our catalysts as a result of the different oxidation pretreatments. The Pt on the deactivated catalysts (fresh or sintered) was on average more oxidized than that on the corresponding active catalysts. This conclusion is supported by both the increase in the amount of oxygen removed by the CO titration per surface Pt from 1.5 to 2.0 and by the small increase in the Pt binding energy in the XPS. Because chemisorption produces an O/Pt_S stoichiometry of 1, the foregoing increases suggest increasing penetration of oxygen into the interior of the Pt particles and an approach to PtO stoichiometry. It is interesting that the XPS data do not support a model of a PtO shell and Pt core, because there is no evidence in the spectra for two distinct phases. One explanation is that at the Pt particle sizes studied, oxygen diffuses into the bulk, producing only one phase as observed by XPS. A particle size analysis by TEM is needed to further analyze this issue. It does appear, however, that when the particle absorbs a critical amount of oxygen, the surface of the particle changes to a lower activity chemical state.

We should emphasize that the oxygen to surface Pt ratios of 1.5 and 2.0 reported here do not necessarily define the number of oxygen layers. To define the position of the oxygen on the Pt clusters using our data, one needs to assume that the oxygen interaction does not depend on particle size and that a compound is formed, not just oxygen dissolved into the bulk.

Because on the deactivated catalysts, the oxygen uptake was about 40% higher than the uptake seen after the NO oxidation reaction, it appears that there is a window of oxygen amount on Pt above which the catalyst is deactivated. Ovesson et al. [31] also found by ab initio kinetic simulations that the catalytic activity of Pt(111) for NO oxidation was sensitive to the oxygen coverage. They found that the surface reaction was endothermic or inhibited in the low-coverage limit but became exothermic only at about 0.25 ML O coverage at temperatures above 400 K due to the lateral repulsive O–O and O–NO interactions. However, O coverage as high as 0.45 ML was required for activation at room temperature. They also found that at high temperatures (400 K and above), the reaction could be driven backward and forward with only slight changes in the O coverage around 0.25 ML, but large changes would be required at low temperatures due to kinetic limitations. Although the above-mentioned study puts a lower limit on the O coverage, our results serve to impose an upper bound on the catalyst's oxygen uptake to keep the catalyst active.

The CO titration curves were also used to compare the rate at which oxygen can be removed from the two catalysts by CO, thereby giving an indication of the reactivity of oxygen on the two catalysts. Under the flow conditions used for the titrations (488 $cm^3\,min^{-1}$), the results are influenced by the flow dynamics of the gas cell of the IR analyzer used for measurements. The residence time in the IR gas cell was ca. 20 s, and the time of titration varied between 1 and 3 min. Thus, the measured CO_2 response was significantly affected by the mixing dynamics of the IR cell. We tried to separate the IR cell mixing effects from the actual reaction process by studying the residence time distribution of the IR cell. The responses to positive and negative step tracer experiments and also to several pulse experiments in the IR analyzer did not follow a regime that we could model. However, because all of the titrations were performed identically, it can be assumed that the titration results are influenced by the mixing dynamics identically, and thus the difference in the CO_2 traces of Fig. 5 on the two catalysts after the various pretreatments can be taken as an indication of the

Table 5
Time constants for the linear rise and exponential decay of CO_2 production rate for the fresh and sintered catalyst during CO titration

Titration following	Catalyst	Linear time constant ($\times 10^{-3}$ s^{-2})	Exponential decay constant ($\times 10^{-3}$ s^{-1})
Pretreatment with O_2	Fresh	5.16 ± 1.10	35.0 ± 0.66
	Sintered	7.15 ± 0.30	56.7 ± 1.94
Pretreatment with reaction mixture	Fresh	1.98 ± 0.07	25.2 ± 0.40
	Sintered	2.90 ± 0.10	36.6 ± 1.20
Pretreatment with deactivation mixture	Fresh	1.59 ± 0.04	24.5 ± 0.50
	Sintered	1.62 ± 0.04	35.2 ± 1.90

Pretreatment conditions as in Table 3.

differing reactivity of the catalysts toward CO. With this IR cell mixing caveat, the simplest model found to describe the CO_2 production rate (or the oxygen removal rate) consisted of two main parts: (i) an initial linear increase in the CO_2 production rate with time until about 10% of the total oxygen is removed and (ii) a near-exponential decay in the CO_2 production rate at later times. The intermediate time region around the peaks of the curves was not fitted. As an example, Fig. 5 shows the linear and exponential fits to the experimental titration data for the fresh catalyst after the NO oxidation reaction.

Table 5 gives the values of the time constants associated with the linear rise and the exponential decay regions and their 95% confidence intervals for each titration experiment on the fresh and sintered catalysts. Simple comparison of these time constants shows a trend toward higher time constants for the sintered catalyst than for the fresh catalyst for all pretreatments. A higher linear time constant implies faster CO_2 formation or oxygen removal rate by CO. Similarly, a higher exponential decay constant also implies a faster removal of oxygen from the catalyst. Thus, the trend seen in the time constants associated with the linear rise and the exponential decay regions indicates that removal of oxygen by CO is easier from the sintered catalyst, which has larger Pt particles, than from the fresh catalyst. This could imply that the interaction of oxygen with larger Pt particles is weaker than that with the smaller particles, in accordance with observations by several researchers [41,42,54]. If this trend were the same in the oxidation of NO to NO_2 over supported Pt, then the increase in the TOR associated with an increase in the metal particle size would be correlated with a decrease in the platinum–oxygen bond strength, as also noted by other researchers [34,35]. This should encourage the development of NO oxidation catalysts with high oxidation resistance. For example, Olsson et al. [24] found that adding an acidic component like vanadia to Pt/TiO_2 catalyst resulted in stable activity for NO oxidation reaction and suggested that the electrophilic vanadia pulls the electron density from platinum, making it more resistant to oxide formation. Similarly, Yazawa et al. [37] concluded that Pt on acidic supports has a higher ability to maintain its metallic state and resist oxidation and hence has higher catalytic activity for propane combustion than Pt on basic supports. Kieken et al. [29] found that increasing the atomic percent of Au from 0 to about 44 on Pt–Au(100) alloy surfaces increased the steady-state decomposition of NO to N_2 under lean operating conditions by decreasing the oxygen binding energy and hence the oxygen coverage under reaction conditions.

5. Conclusion

The reaction kinetics of NO oxidation and the deactivation behavior for two Pt/Al_2O_3 catalysts having different dispersions have been investigated. The TOR on the sintered catalyst having a Pt cluster size of 7.0 nm was ca. 4 times higher than the TOR on the fresh catalyst with a size of 2.4 nm. Based on experiments designed using a central composite design (CCD) for the fresh catalyst, we calculated apparent kinetic parameters that matched our previously published results on NO oxidation kinetics for the same catalyst [33] investigated by the one-at-a-time variation of parameters method. The CCD statistical design probed for interactions among the variables and showed that the apparent kinetic parameters were valid for all combinations of parameters in the range of temperatures and concentrations tested. The reaction was nearly first order in both NO and O_2 and nearly negative first order in NO_2, and the apparent activation energy was 81.8 ± 5 kJ mol^{-1}. The rate of NO oxidation on the sintered catalyst had a similar order dependence with respect to both NO and NO_2 concentrations and also had similar apparent activation energy as the fresh catalyst. However, the apparent O_2 order was ca. 0.7, a lower value compared with the near-first-order dependence observed for the fresh catalyst. Both fresh and sintered catalysts were found to deactivate when exposed to conditions that favored Pt oxide formation: low temperature and the strong oxidant NO_2. The oxygen uptake by Pt on these catalysts after NO oxidation reaction and after deactivation by exposure to NO_2 was quantified using the CO titration method. It was found that the oxygen uptake after NO oxidation reaction and also after catalyst deactivation was proportional to the exposed surface area of platinum on the two Pt particle sizes tested. The oxygen uptake was found to be 1.5 and 2 times the amount of Pt on the surface after reaction and deactivation, respectively, for both catalysts. XPS measurements also showed similar shifts in the Pt binding energy on both catalysts, after NO oxidation reaction and after their deactivation, supporting the presence of only one phase. The activity of these deactivated catalysts could be completely restored by mild exposure to CO or H_2. Based on the XPS and CO titration measurements, the observed catalyst deactivation was attributed to an increase in bulk oxidation of the Pt particles toward PtO that is sufficient to alter the surface to a less active state. Titration results using CO also show that the higher NO oxidation TOR observed on large Pt particles may be due to their weaker interaction with oxygen compared with small particles.

Acknowledgments

The authors thank the Indiana 21st Century Research and Technology Fund and Cummins, Inc. for financial support of this work. They also acknowledge support from the U.S. Department of Energy (CRADA ORNL97-0489).

References

[1] Control of air pollution from new motor vehicles: Heavy-duty engine and vehicle standards and highway diesel fuel sulfur control requirements, US EPA, 40 CFR Part 69, 80 and 86.
[2] R. Burch, J.A. Sullivan, T.C. Watling, Catal. Today 42 (1998) 13.
[3] C. Yokoyama, M. Misono, J. Catal. 150 (1994) 9.
[4] H. Hamada, Y. Kintaichi, M. Inaba, M. Tabata, T. Yoshinari, H. Tsuchida, Catal. Today 29 (1996) 53.
[5] H. Ohtsuka, Appl. Catal. B 33 (2001) 325.
[6] J. Despres, M. Elsener, M. Koebel, O. Kroecher, B. Schnyder, A. Wokaun, Appl. Catal. B 50 (2004) 73.
[7] N. Takahashi, H. Shinjoh, T. Iijima, T. Suzuki, K. Yamazaki, K. Yokota, H. Suzuki, N. Miyoshi, S.-i. Matsumoto, et al., Catal. Today 27 (1996) 63.
[8] W.S. Epling, L.E. Campbell, A. Yezerets, N.W. Currier, J.E. Parks, Catal. Rev. 46 (2004) 163.
[9] K.S. Kabin, R.L. Muncrief, M.P. Harold, Y. Li, Chem. Eng. Sci. 59 (2004) 5319.
[10] S. Salasc, M. Skoglundh, E. Fridell, Appl. Catal. B 36 (2002) 145.
[11] H. Mahzoul, J.F. Brilhac, P. Gilot, Appl. Catal. B 20 (1999) 47.
[12] F. Prinetto, G. Ghiotti, I. Nova, L. Lietti, E. Tronconi, P. Forzatti, J. Phys. Chem. B 105 (2001) 12732.
[13] S. Kikuyama, I. Matsukuma, R. Kikuchi, K. Sasaki, K. Eguchi, Appl. Catal. A 226 (2002) 23.
[14] P.J. Schmitz, R.J. Baird, J. Phys. Chem. B 106 (2002) 4172.
[15] B.J. Cooper, H.J. Jung, J.E. Thos, US Patent 4,902,487 (1990).
[16] J.-H. Lee, H.H. Kung, Catal. Lett. 51 (1998) 1.
[17] L. Olsson, B. Westerberg, H. Persson, E. Fridell, M. Skoglundh, B. Andersson, J. Phys. Chem. B 103 (1999) 10433.
[18] G. Corro, M.P. Elizalde, A. Velasco, React. Kinet. Catal. Lett. 76 (2002) 117.
[19] R. Marques, P. Darcy, P. Da Costa, H. Mellottee, J.-M. Trichard, G. Djega-Mariadassou, J. Mol. Catal. A: Chem. 221 (2004) 127.
[20] E. Xue, K. Seshan, J.R.H. Ross, Appl. Catal. B 11 (1996) 65.
[21] E. Xue, K. Seshan, J.G. van Ommen, J.R.H. Ross, Appl. Catal. B 2 (1993) 183.
[22] J. Oi-Uchisawa, A. Obuchi, R. Enomoto, S. Liu, T. Nanba, S. Kushiyama, Appl. Catal. B 26 (2000) 17.
[23] S.S. Mulla, N. Chen, L. Cumaranatunge, W.N. Delgass, W.S. Epling, F.H. Ribeiro, Catal. Today 114 (2006) 57.
[24] L. Olsson, M. Abul-Milh, H. Karlsson, E. Jobson, P. Thormaehlen, A. Hinz, Top. Catal. 30/31 (2004) 85.
[25] R. Burch, T.C. Watling, J. Catal. 169 (1997) 45.
[26] P. Denton, A. Giroir-Fendler, H. Praliaud, M. Primet, J. Catal. 189 (2000) 410.
[27] M. Crocoll, S. Kureti, W. Weisweiler, J. Catal. 229 (2005) 480.
[28] M. Crocoll, W. Weisweiler, Chem. Ing. Tech. 76 (2004) 1490.
[29] L.D. Kieken, M. Neurock, D. Mei, J. Phys. Chem. B 109 (2005) 2234.
[30] D. Mei, Q. Ge, M. Neurock, L. Kieken, J. Lerou, Mol. Phys. 102 (2004) 361.
[31] S. Ovesson, B.I. Lundqvist, W.F. Schneider, A. Bogicevic, Phys. Rev. B 71 (2005).
[32] W.F. Schneider, in: V.H. Grassian (Ed.), Environmental Catalysis, Marcel–Dekker, 2005.
[33] S.S. Mulla, N. Chen, W.N. Delgass, W.S. Epling, F.H. Ribeiro, Catal. Lett. 100 (2005) 267.
[34] L. Olsson, E. Fridell, J. Catal. 210 (2002) 340.
[35] S. Benard, L. Retailleau, F. Gaillard, P. Vernoux, A. Giroir-Fendler, Appl. Catal. B 55 (2005) 11.
[36] E. Fridell, A. Amberntsson, L. Olsson, A.W. Grant, M. Skoglundh, Top. Catal. 30/31 (2004) 143.
[37] Y. Yazawa, N. Kagi, S.-i. Komai, A. Satsuma, Y. Murakami, T. Hattori, Catal. Lett. 72 (2001) 157.
[38] N. Hartmann, R. Imbihl, W. Vogel, Catal. Lett. 28 (1994) 373.
[39] B.L.M. Hendriksen, J.W.M. Frenken, Phys. Rev. Lett. 89 (2002) 046101/1.
[40] J. Dicke, H.H. Rotermund, J. Lauterbach, Surf. Sci. 454–456 (2000) 352.
[41] M.N. Padilla-Serrano, F.J. Maldonado-Hodar, C. Moreno-Castilla, Appl. Catal. B 61 (2005) 253.
[42] P. Briot, A. Auroux, D. Jones, M. Primet, Appl. Catal. 59 (1990) 141.
[43] J.E. Benson, M. Boudart, J. Catal. 4 (1965) 704.
[44] D.C. Montgomery, G.C. Runger, Applied Statistics and Probability for Engineers, Wiley, New York, 2003, p. 14.
[45] F.H.M. Dekker, A. Bliek, F. Kapteijn, J.A. Moulijn, Chem. Eng. Sci. 50 (1995) 3573.
[46] C.D. Wagner, W.M. Riggs, L.E. Davis, J.F. Moulder, G.E. Muilenberg, Handbook of X-Ray Photoelectron Spectroscopy, Perkin–Elmer Corporation, Eden Prairie, MN, 1979, p. 50.
[47] S. Doniach, M. Sunjic, J. Phys. B 3 (1970) 285.
[48] D.A. Shirley, Phys. Rev. B [3] 5 (1972) 4709.
[49] J.Z. Shyu, K. Otto, Appl. Surf. Sci. 32 (1988) 246.
[50] T. Huizinga, H.F.J. Van't Blik, J.C. Vis, R. Prins, Surf. Sci. 135 (1983) 580.
[51] A. Talo, J. Lahtinen, P. Hautojarvi, Appl. Catal. B 5 (1995) 221.
[52] L. Olsson, H. Persson, E. Fridell, M. Skoglundh, B. Andersson, J. Phys. Chem. B 105 (2001) 6895.
[53] M. Boudart, A. Aldag, J.E. Benson, N.A. Dougharty, C. Girvin Harkins, J. Catal. 6 (1966) 92.
[54] E.S. Putna, J.M. Vohs, R.J. Gorte, Surf. Sci. 391 (1997) L1178.
[55] W.A. Brown, R. Kose, D.A. King, Chem. Rev. 98 (1998) 797.
[56] R.J. Berry, Surf. Sci. 76 (1978) 415.
[57] J. Segner, W. Vielhaber, G. Ertl, Isr. J. Chem. 22 (1982) 375.
[58] D.H. Parker, B. Koel, J. Vac. Sci. Technol. A 8 (1990) 2585.
[59] R.W. McCabe, C. Wong, H.S. Woo, J. Catal. 114 (1988) 354.
[60] P. Legare, Surf. Sci. 580 (2005) 137.
[61] J.F. Weaver, J.-J. Chen, A.L. Gerrard, Surf. Sci. 592 (2005) 83.
[62] C.-P. Hwang, C.-T. Yeh, J. Mol. Catal. A: Chem. 112 (1996) 295.
[63] C.-B. Wang, C.-T. Yeh, J. Catal. 178 (1998) 450.